

Squeezed light for advanced gravitational wave detectors and beyond

E. Oelker,^{*1} L. Barsotti,¹ S. Dwyer,² D. Sigg,² and N. Mavalvala¹

¹ LIGO - Massachusetts Institute of Technology, Cambridge, MA 02139, USA

² LIGO - Hanford Observatory, Richland, WA 99352, USA

*oelker@mit.edu

Abstract: Recent experiments have demonstrated that squeezed vacuum states can be injected into gravitational wave detectors to improve their sensitivity at detection frequencies where they are quantum noise limited. Squeezed states could be employed in the next generation of more sensitive advanced detectors currently under construction, such as Advanced LIGO, to further push the limits of the observable gravitational wave Universe. To maximize the benefit from squeezing, environmentally induced disturbances such as back scattering and angular jitter need to be mitigated. We discuss the limitations of current squeezed vacuum sources in relation to the requirements imposed by future gravitational wave detectors, and show a design for squeezed light injection which overcomes these limitations.

© 2014 Optical Society of America

OCIS codes: (270.6570) Squeezed States; (120.3180) Interferometry; (350.1270) Astronomy and astrophysics; (190.4970) Parametric oscillators and amplifiers; (270.2500) Fluctuations, relaxations, and noise; (290.1350) Backscattering.

References and links

1. G. M. Harry (for the LIGO Scientific Collaboration), "Advanced LIGO: the next generation of gravitational wave detectors," *Class. and Quant. Grav.* **27**, 084006 (2010).
2. Virgo Collaboration, "Advanced Virgo status", *Proceeding of the 9th LISA symposium* (2012).
3. Y. Aso, Y. M.chimura, K. Somiya, M. Ando, O. Miyakawa, T. Sekiguchi, D. Tatsumi, and H. Yamamoto, "Interferometer design of the KAGRA gravitational wave detector," *Phys. Rev. D* **88**, 043007 (2013).
4. The LIGO Scientific Collaboration, "LIGO: the Laser Interferometer Gravitational-Wave Observatory," *Rep. Prog. Phys.* **72**, 076901 (2009).
5. Virgo Collaboration, "Virgo: a laser interferometer to detect gravitational waves," *Journal of Instrumentation* **7**, P03012 (2012).
6. H. Grote and the LIGO Scientific Collaboration, "The GEO600 status," *Class. and Quant. Grav.* **27**, 084003 (2010).
7. K. McKenzie, N. Grosse, W. P. Bowen, S. Whitcomb, M. Gray, D. McClelland, and P. K. Lam, "Squeezing in the audio gravitational wave detection band," *Phys. Rev. Lett.* **93**, 161105 (2004).
8. H. Vahlbruch, S. Chelkowski, B. Hage, A. Franzen, K. Danzmann, and R. Schnabel, "Coherent control of vacuum squeezing in the gravitational-wave detection band," *Phys. Rev. Lett.* **97**, 011101 (2006).
9. H. Vahlbruch, S. Chelkowski, K. Danzmann, and R. Schnabel, "Quantum engineering of squeezed states for quantum communication and metrology," *New J. Phys.* **9**, 371 (2007).
10. K. Goda, O. Miyakawa, E. E. Mikhailov, S. Saraf, R. Adhikari, K. McKenzie, R. Ward, S. Vass, A. J. Weinstein, and N. Mavalvala, "A quantum-enhanced prototype gravitational-wave detector," *Nature Phys.* **4**, 472 (2008).
11. The LIGO Scientific Collaboration, "A gravitational wave observatory operating beyond the quantum shot-noise limit," *Nature Phys.* **7**(12), 962–965 (2011).
12. The LIGO Scientific Collaboration, "Enhanced sensitivity of the LIGO gravitational wave detector by using squeezed states of light," *Nature Photon.* **7**, 613–619 (2013).
13. S. Dwyer, L. Barsotti, S. S. Y. Chua, M. Evans, M. Factourovich, D. Gustafson, T. Isogai, K. Kawabe, A. Khalidovskii, P. K. Lam, M. Landry, N. Mavalvala, D. E. McClelland, G. D. Meadors, C. M. Mow-Lowry, R.

- Schnabel, R. M. S. Schofield, N. Smith-Lefebvre, M. Stefszky, C. Vorvick, and D. Sigg, "Squeezed quadrature fluctuations in a gravitational wave detector using squeezed light," *Opt. Express* **21**, 19047–19060 (2013).
14. S. Chua, S. Dwyer, L. Barsotti, D. Sigg, R. Schofield, V. Frolov, K. Kawabe, M. Evans, G. Meadors, M. Factourovich, R. Gustafson, N. Smith-Lefebvre, C. Vorvick, M. Landry, A. Khalaidovski, M. Stefszky, C. Mow-Lowry, B. Buchler, D. Shaddock, P. K. Lam, R. Schnabel, N. Mavalvala, and D. E. McClelland, "Impact of back scattered light in a squeezing-enhanced interferometric gravitational wave detector," *Class. and Quant. Grav.* **31**, 035017 (2014).
 15. M. Evans, L. Barsotti, P. Kwee, J. Harms, and H. Miao, "Realistic filter cavities for advanced gravitational wave detectors," *Phys. Rev. D* **88**, 022002 (2013).
 16. R. X. Adhikari, "Gravitational radiation detection with laser interferometry," *Rev. Mod. Phys.* **86**, 121 (2014).
 17. E.T. Collaboration, "The Einstein Telescope: a third-generation gravitational wave observatory," *Class. and Quant. Grav.* **27**(19), 194002 (2010).
 18. The LIGO Scientific Collaboration, "Predictions for the rates of compact binary coalescences observable by ground-based gravitational-wave detectors," *Class. and Quant. Grav.* **27**, 173001 (2010).
 19. The LIGO Scientific Collaboration, "Search for gravitational waves from low mass compact binary coalescence in LIGO's sixth science run and Virgo's science runs 2 and 3," *Phys. Rev. D* **85**, 082002 (2012).
 20. M. S. Stefszky, C. M. Mow-Lowry, S. S. Y. Chua, D. A. Shaddock, B. C. Buchler, H. Vahlbruch, A. Khalaidovski, R. Schnabel, P. K. Lam, and D. E. McClelland, "Balanced homodyne detection of optical quantum states at audio-band frequencies and below," *Class. and Quant. Grav.* **29**, 145015 (2012).
 21. T. Eberle, S. Steinlechner, J. Bauchrowitz, V. Handchen, H. Vahlbruch, M. Mehmet, H. Muller-Ebhardt, and R. Schnabel, "Quantum enhancement of the zero-area sagnac interferometer topology for gravitational wave detection," *Phys. Rev. Lett.* **104**, 251102 (2010).
 22. A. Khalaidovski, "Beyond the quantum limit: a squeezed-light laser in GEO600," PhD. Thesis, University of Hannover (2012).
 23. R. W. P. Drever, J. L. Hall, F. V. Kowalski, J. Hough, G. M. Ford, A. J. Munley, and H. Ward, "Laser phase and frequency stabilization using an optical resonator," *Appl. Phys. B* **31**(2), 97 (1983).
 24. D. Anderson, "Alignment of resonant optical cavities," *Appl. Opt.* **23**, 2944–2949 (1984).
 25. S. Dwyer, "Quantum noise reduction using squeezed states in LIGO," PhD. Thesis, Massachusetts Institute of Technology (2012).
 26. B. Canuel, E. Genin, G. Vajente, and J. Marque, "Displacement noise from back scattering and specular reflection of input optics in advanced gravitational wave detectors," *Opt. Express* **21**(9), 10546–10562 (2013).
 27. P. Kwee, J. Miller, T. Isogai, L. Barsotti, and M. Evans, "Decoherence and degradation of squeezed states in quantum filter cavities," submitted for publication (2014)
 28. S. Chua, M. Stefszky, C. Mow-Lowry, B. Buchler, S. Dwyer, D. Shaddock, P. K. Lam, and D. McClelland, "Backscatter tolerant squeezed light source for advanced gravitational-wave detectors," *Opt. Lett.* **36**(23), 4680 (2011).
 29. M. Kasprzack, B. Canuel, F. Cavalier, R. Day, E. Genin, J. Marque, D. Sentenac, and G. Vajente, "Performance of a thermally deformable mirror for correction of low-order aberrations in laser beams," *Appl. Opt.* **52**(12), 2909–2916 (2013).
 30. Z. Liu, P. Fulda, M. A. Arain, L. Williams, G. Mueller, D. B. Tanner, and D. H. Reitze, "Feedback control of optical beam spatial profiles using thermal lensing," *Appl. Opt.* **52**(26), 6452–6457 (2013)
 31. F. Magaa-Sandoval, R. Adhikari, V. Frolov, J. Harms, J. Lee, S. Sankar, P. Saulson, and J. Smith, "Large-angle scattered light measurements for quantum-noise filter cavity design studies," *JOSA A* **29**(8), 1722–1727 (2012).
 32. T. Isogai, J. Miller, P. Kwee, L. Barsotti, and M. Evans, "Loss in long-storage-time optical cavities," *Opt. Express* **21**(24), 30114–30125 (2013).
 33. H. Grote, K. Danzmann, K. Dooley, R. Schnabel, J. Slutsky, and H. Vahlbruch, "First long-term application of squeezed states of light in a gravitational-wave observatory," *Phys. Rev. Lett.* **110**, 181101 (2013).
 34. K. Dooley, "Phase control of squeezed states of light in gravitational-wave detectors," in preparation.
 35. E. Schreiber, "Alignment sensing and control for squeezed vacuum states of light," in preparation.
 36. S. Hild, H. Grote, J. Degallaix, S. Chelkowski, K. Danzmann, A. Freise, M. Hewitson, J. Hough, H. Luck, M. Prijatelj, K.A. Strain, J. R. Smith, and B. Willke, "DC readout of signal-recycled gravitational wave detector," *Class. Quantum Grav.* **26**, 055012, 2009
 37. T. T. Fricke, N. D. Smith-Lefebvre, R. Abbott, R. Adhikari, K. L. Dooley, M. Evans, P. Fritschel, V. V. Frolov, K. Kawabe, J. S. Kissel, B. J. J. Slagmolen, and S. J. Waldman, "DC readout experiment in enhanced LIGO," *Class. and Quant. Grav.* **29**, 065005 (2012).
 38. K. Arai, S. Barnum, P. Fritschel, J. Lewis, and S. Waldman, "Output mode cleaner design," LIGO working note, LIGO-T1000276-v5 (2013).
 39. M. Notcutt, L. Ma, A. D. Ludlow, S. Foreman, J. Ye, and J. L. Hall, "Contribution of thermal noise to frequency stability of rigid optical cavity via Hertz-linewidth lasers," *Phys. Rev. A* **73**, 031804 (2006)
 40. H. Vahlbruch, S. Chelkowski, B. Hage, A. Franzen, K. Danzmann, and R. Schnabel, "Coherent control of vacuum squeezing in the gravitational-wave detection band," *Phys. Rev. Lett.* **97**, 011101 (2006).
 41. S. Chelkowski, H. Vahlbruch, K. Danzmann, and R. Schnabel, "Coherent control of broadband vacuum squeez-

- ing,” *Phys. Rev. A* **75**, 043814 (2007).
42. F. Matichard, “LIGO vibration isolation and alignment platforms: an overview of systems, features and performance of interest for the field of precision positioning and manufacturing,” *Proceedings of ASPE conference on Precision Control for Advanced Manufacturing Systems*, (2013).
-

1. Introduction

A global network of kilometer scale interferometers is currently being built with the aim of detecting gravitational waves [1–3]. These second generation detectors, such as Advanced LIGO, will be about 10 times more sensitive than their predecessors [4–6], measuring displacements on the order of $10^{-20}\text{m}/\sqrt{\text{Hz}}$ at 100 Hz.

By circulating almost a megawatt of light power in each arm cavity, advanced detectors will be limited by quantum noise in their entire detection band, though thermal noise contributes significantly below 100 Hz. Further increasing the circulating power to reduce quantum noise will be extremely challenging, due to thermal effects caused by light absorption. Over the last decade, the injection of squeezed states of light has emerged as a viable alternative route to push the sensitivity of gravitational wave detectors beyond the quantum limit [7–10]. Squeezed enhancement in first-generation of gravitational wave detectors was first demonstrated at the GEO600 detector, with a maximal improvement in signal to noise ratio of 3.5 dB at frequencies above about 700 Hz [11]. Shortly thereafter the LIGO H1 detector showed up to 2.1 dB improvement at frequencies above 150 Hz [12].

The upcoming generation of gravitational wave detectors imposes stricter constraints on the squeezed light source than its predecessors. The purpose of this paper is to establish the requirements for an advanced squeezed light source, compare these requirements to what has been achieved to date, and to propose a design that closes the gap between the two. Our proposed design aims to maximize the benefit from squeezing by minimizing the impact of known noise sources, such as optical losses, phase noise and back scattered noise [13, 14]. When integrated with quantum filter cavities [15], this solution allows us to achieve a broadband reduction of quantum noise in advanced detectors, that is also suitable for the third generation of detectors envisioned for the next decade [16, 17]. Realizing greater levels of squeezing at any frequency allows gravitational wave detectors to probe an observation volume that increases as the cube of the sensitivity improvement [18]. Moreover, pushing the squeezing enhancement to lower frequencies is critical for early detection of coalescing compact binaries [19].

2. Limits to effective squeezing

The amount of effective squeezing that can be measured in any optical system limited by quantum noise is determined by how much squeezing is injected into the apparatus, by the losses in the apparatus, and by squeezed quadrature fluctuations, also known as phase noise (see for instance [13] and references therein). Losses reduce the level of measured squeezing by mixing in ordinary vacuum with the squeezed field. Squeezed quadrature fluctuations about a mean quadrature angle – or phase noise – arises from relative fluctuations between the squeezed quadrature and the measured quadrature. These fluctuations project noise from the anti-squeezed quadrature into the measurement. Moreover, scattered light can add noise to the squeezed field, reducing the level of measured squeezing.

Figure 1 shows how squeezed quadrature fluctuations and optical losses determine the maximum amount of effective squeezing.

For optical losses of 30% or more, squeezed quadrature fluctuations could be as high as tens of mrad without significantly reducing the maximum level of squeezing [13]. However, the sensitivity to squeezed quadrature fluctuations increases as the optical losses are reduced.

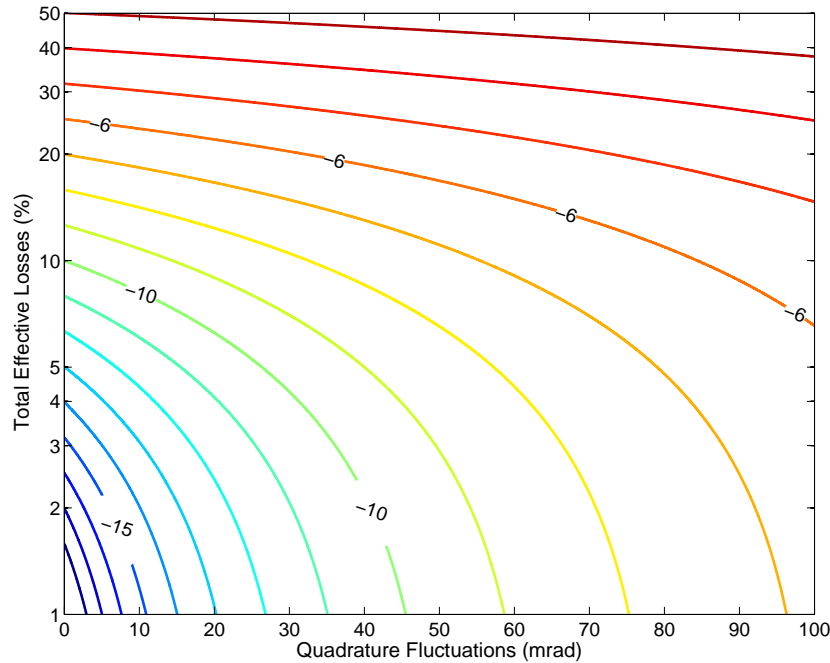


Fig. 1: Maximum level of “effective” squeezing measurable in an optical system in the presence of optical losses and squeezed quadrature fluctuations, obtained by optimizing the amount of input squeezing [13]. Squeezing levels relative to shot noise are expressed in decibels. The squeezed quadrature fluctuations are root mean squared (RMS) fluctuations about a mean quadrature angle chosen to maximize the level of squeezing.

For instance, 10% to 15% losses allow for -8 to -10 dB of squeezing provided that squeezed quadrature fluctuations are reduced to a few milliradians.

A simplified schematic of squeezed light injection in a first generation gravitational wave detector is shown in the top panel of Fig. 2. The squeezed light source is located outside the interferometer’s vacuum envelope. A sub-threshold optical parametric oscillator (OPO) is pumped with light at 532 nm to produce squeezed vacuum at 1064 nm via parametric downconversion in a second-order nonlinear PPKTP crystal. In the case of the LIGO squeezing demonstration (Ref. [12]), a 0.28 meter free-space bow-tie OPO cavity with the nonlinear crystal placed at a beam waist of $30\ \mu\text{m}$ is used [28]. Squeezed vacuum is injected into the interferometer through the Output Faraday Isolator. It is then reflected back toward the Output Mode Cleaner (OMC), and together with the interferometer beam reaches the Output Photodiode that measures the gravitational wave signal through homodyne detection [37].

Specific details of the squeezed light sources employed so far in gravitational wave detectors can be found in [11, 12]. In general, the relative phase between the interferometer and squeezed fields is controlled by using the *coherent control* technique [40, 41]. A single RF “control” sideband at frequency $f_0 - \Omega$, with detuning Ω with respect to the “pump laser” frequency f_0 , is injected into the OPO. In the presence of an intense pump field at twice the laser frequency $2f_0$, this sideband undergoes difference frequency generation which produces a second sideband with the opposite detuning, $f_0 + \Omega$. Both the squeezed field and the control sidebands are injected into the interferometer and return along with the interferometer field. Along the readout path, a small sample of the light is picked-off to measure the interference between in-

terferometer and control fields. Demodulation of this interference signal at Ω allows us to lock the relative phase (*squeezing angle*) between the squeezed field and the interferometer field by actuating on the pump laser frequency.

Connecting a squeezed vacuum source to the output port of a gravitational wave interferometer opens another port that may introduce scattered light [14]. Light exiting the interferometer from the Output Faraday Isolator toward the squeezed light source can scatter off of moving surfaces in the squeezing injection path and propagate to the interferometer readout photodetector, degrading the detector sensitivity in the audio frequency band. One additional Faraday Isolator (Squeezing Injection Faraday Isolator, in top panel of Fig. 2) is placed in between the squeezed light source and the interferometer to mitigate the impact of back scattered light noise. Although both the GEO600 and LIGO squeezing demonstrations were able to mitigate backscatter well enough to demonstrate squeezing without degrading the detector's strain spectrum, the total noise of these first generation interferometers was at least a factor of 50 above quantum noise at frequencies below 50 Hz [11, 12], while in advanced detectors quantum noise will be a dominant noise source in the entire detection band down to 10 Hz [1].

In the sections that follow we describe the origin of these noise sources, and explain how they can be overcome to maximize squeezing enhancement in future gravitational wave detectors. Specifically, we discuss *losses* arising from the optical train and from misaligned optical fields in Section 3. In Section 4 we address *quadrature angle fluctuations* arising from fluctuations in the OPO length and alignment jitter. In Section 5 we will discuss how to control *scattered light*. In Section 6 we evaluate the impact of these noise sources on Advanced LIGO and *present a design* for a squeezed light source that can satisfy the stringent requirements of advanced detectors.

3. Losses

Quantum states are fragile and, therefore, easily degraded by losses in the optical system. We consider two mechanisms that give rise to substantial losses.

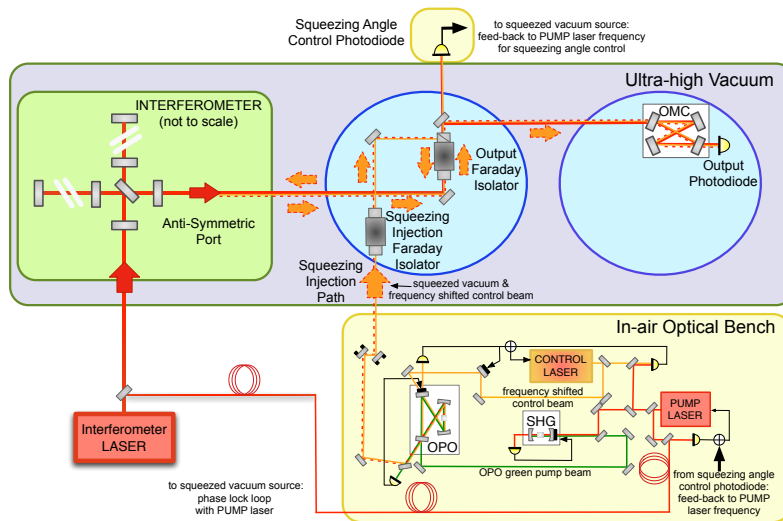
3.1. Optical losses

The squeezed beam experiences losses in the optical path from the squeezed light source to the interferometer readout photodetector (see Fig. 2). These losses are typically caused by imperfections in optical surfaces and polarizing optics (such as Faraday Isolators), and by imperfect spatial overlap (*mode matching*) when coupling the beam to resonant cavities such as the OMC. In table top squeezing experiments, total losses of 10% or less have been realized, yielding squeezing enhancement of more than 10 dB [20, 21].

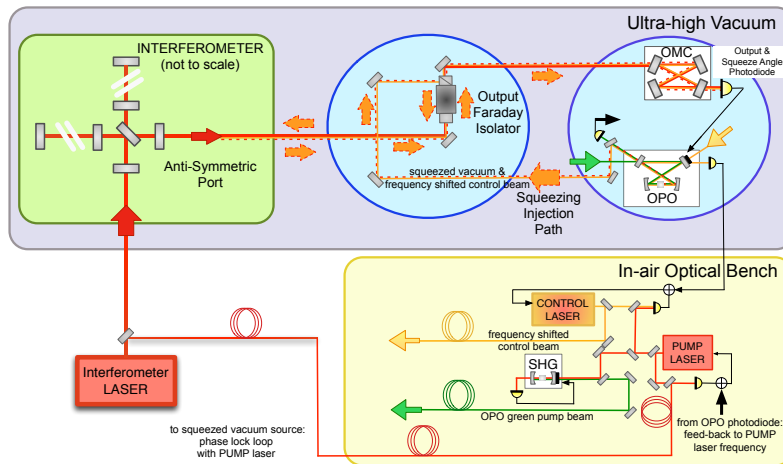
However, in large scale interferometers there are additional optical components and resonant cavities in between the squeezed light source and the interferometer readout, and the losses are typically much higher. In the GEO600 and LIGO H1 squeezing demonstrations [11, 12], optical losses of 38% and 56% respectively were measured, limiting the squeezing enhancement to 3.5 dB and 2.1 dB. Some of the losses were due to particular limitations of the experimental setups; total losses of 20-30% should be readily achievable in advanced detectors, allowing for 6 dB of noise reduction using squeezing. Reducing the losses down to the 10% level will require additional effort to limit the loss from each source, and will allow for 10 dB of noise reduction due to squeezing, as will be detailed in section 6.

3.2. Losses induced by alignment fluctuations

Alignment fluctuations of the squeezed field also introduce losses by reducing the coupling through the OMC or arm cavities. A misalignment or displacement of the squeezed beam on a



(a) Top



(b) Bottom

Fig. 2: **Top:** A typical set-up for squeezing injection in the first demonstrations of squeezing at GEO600 and LIGO, both using DC readout [36, 37]. The shaded gray region corresponds to the detector vacuum envelope; the cyan circles represent seismically isolated tables. The squeezed light source is housed outside of vacuum. The OPO cavity is locked to the green pump light. The squeezed (dashed red) and control (orange) fields enter vacuum through a viewport and are injected into the interferometer through the Output Faraday Isolator. A Squeezing Injection Faraday Isolator is inserted between the squeezed light source and the Output Faraday to provide additional attenuation of backscattered light [11, 14]. A small pickoff beam is sampled prior to the output mode cleaner (OMC) to control the squeezed quadrature angle. The squeezed and interferometer fields are measured in transmission through the OMC to obtain the gravitational wave signal. Details of the control topologies adopted in first generation detectors can be found in [11, 12]. **Bottom:** Proposed design for future detectors. This design features an in-vacuum OPO. The remainder of the squeezed light source remains outside of vacuum. The coherent control error signal [8] is now derived in transmission through the OMC [33]. Details of this new control topology can be found in section 6.

steering optic in between the OPO and the asymmetric port of the interferometer reduces the power in the TEM_{00} mode [24] and it is equivalent to a loss L

$$L \simeq \left(\frac{\tilde{\theta}_x \omega_0 \pi}{\lambda} \right)^2 + \left(\frac{\tilde{\Delta}x}{\omega_0} \right)^2 \quad (1)$$

where ω_0 is the beam waist (radius) and $\tilde{\theta}_x$ and $\tilde{\Delta}x$ are the RMS values for the fluctuations in beam angle and displacement, respectively. The beam waist will vary from approximately $\omega_0 = 100 \mu\text{m}$ in the OPO to $\omega_0 = 1 \text{ mm}$ at the asymmetric port of the interferometer where the beam is injected. Equation 1 can be written as

$$L \simeq 0.01 \times \left[\left(\frac{0.3 \tilde{\theta}_x}{100 \mu\text{rad}} \right)^2 + \left(\frac{\tilde{\Delta}x}{10 \mu\text{m}} \right)^2 \right] \quad \text{for } \omega_0 = 100 \mu\text{m} \quad (2)$$

$$L \simeq 0.01 \times \left[\left(\frac{0.3 \tilde{\theta}_x}{10 \mu\text{rad}} \right)^2 + \left(\frac{\tilde{\Delta}x}{100 \mu\text{m}} \right)^2 \right] \quad \text{for } \omega_0 = 1 \text{ mm} \quad (3)$$

To keep the losses below 1% ($L < 0.01$) the displacement of the squeezed beam on the steering optics need to be reduced to less than $10 \mu\text{m}$ RMS where the beam is small, and angular jitter needs to be reduced to less than $30 \mu\text{rad}$ RMS where the beam is large. Meeting these requirements on an in air table without seismic and acoustic isolation can be challenging. Because previous squeezing demonstrations in gravitational wave detectors were dominated by optical losses (see 3.1), losses induced by alignment fluctuations were negligible. However, they must be taken into account when aiming to reduce the total losses down to 10%.

4. Quadrature fluctuations

Many mechanisms have been identified which cause fluctuations in the squeezing angle, also known as quadrature fluctuations ([13] and references therein), such as OPO length noise, drifts in the relative alignment between the squeezed field and the interferometer field, fluctuations in the circulating pump power and noise induced by modulation RF sidebands used to control the interferometer.

The LIGO H1 control scheme was designed to suppress quadrature fluctuations by relying on high bandwidth feedback from the squeezing angle control photodiode to the frequency of the pump laser (see Fig. 2). However, this control scheme is not optimal. For an interferometer with Fabry-Perot arm cavities, the bandwidth of the squeezing angle control loop is limited by the arm cavity free-spectral-range. The 4 km long arm cavities of LIGO have a free spectral range of 37.5 kHz. They are operated on resonance for the interferometer carrier field while the detuning of the squeezing control field, Ω , is tuned to be anti-resonant in the arm cavities. Quadrature fluctuations at frequency ω_a will impress audio sidebands on the control field with detuning $\Omega + \omega_a$. When $\Omega + \omega_a$ is an integer multiple of 37.5 kHz these sidebands become resonant in the arm cavities which will shift their phase relative to the control field. These phase shifted sidebands can cause instabilities in the squeezing angle control loop if they are within the servo bandwidth. This effect was indeed observed during the LIGO H1 squeezing experiment, limiting the squeeze angle control bandwidth to 10 kHz [25].

Moreover, the coherent control technique is susceptible to lock point errors which can limit its ability to suppress phase noise. Fluctuations in the OPO cavity length and drift in the relative alignment between the interferometer and squeezed fields generate lock point errors, as will be detailed in the sections that follow. These lead to significant squeezed quadrature fluctuations even within the control bandwidth.

4.1. Quadrature fluctuations due to OPO length noise

In an OPO cavity, fluctuations in the cavity length lead to phase noise on the squeezed field exiting the cavity. These phase fluctuations will result in fluctuations of the measured quadrature phase at the interferometer readout.

Both implementations of squeezing enhancement in gravitational wave detectors [11, 12] used OPO cavities that were exposed to air currents and the ambient acoustic environment of the laboratory. With little isolation, environmental vibrations led to fluctuations in the length of the OPO cavity, and consequently to quadrature fluctuations.

For an OPO cavity where the pump field is used for Pound-Drever-Hall locking [23], a closed-form expression for the contribution of the OPO length noise to the total quadrature fluctuations is [13]:

$$\frac{d\theta_{sqz}}{d\delta L} = \frac{\omega}{\bar{L}} \left(\frac{1}{\gamma_b^{ot}} + \frac{1}{\gamma_a^{ot}(1+x^2)} \right). \quad (4)$$

Here ω is the frequency of the squeezed field, \bar{L} is the OPO cavity length at zero detuning, γ_b^{ot} is the half width half maximum (HWHM) frequency for the pump field, γ_a^{ot} is the HWHM frequency for the fundamental (squeezed) field, and x is the normalized nonlinear interaction strength ($x = 1 - 1/\sqrt{g}$ where g is the parametric gain).

The coherent control error signal measures phase of the control sidebands relative to the interferometer field, and works on the assumption that the control field responds in the same way to disturbances as the audio frequency sidebands that make up the squeezed field. However, because coherent sidebands are typically detuned from the OPO resonance by more than 10 MHz, they respond differently than the squeezed field does to changes in the cavity length. In the LIGO squeezing experiment, this meant that the coherent control scheme only corrected for half of the quadrature fluctuations due to cavity length fluctuations [13]. While the control field detuning could be lowered to improve the accuracy of the error signal, it must remain large enough to avoid contaminating the squeezed field. The most effective way to reduce these quadrature fluctuations is to reduce the cavity length fluctuations themselves. Quadrature fluctuations due to OPO length noise in the LIGO squeezing demonstration were measured to be 25 mrad RMS [13], however smaller total phase noise (on the order of 5 to 10 mrad) has been measured with OPOs outside of vacuum [20–22].

4.2. Quadrature fluctuations due to alignment jitter

The approach used in [11, 12] to lock the squeezing angle was to pick off a sample of the interferometer output field using a beamsplitter inserted before the OMC and measure its interference with the control field (see Fig. 2). At the squeezing angle control photodetector both fields contain higher order modes TEM_{ij} that have phase offsets relative to the TEM_{00} mode which we will denote as ϕ_{ij}^{ifo} and ϕ_{ij}^{clf} for the interferometer and coherent locking control fields, respectively. When there is a relative misalignment between the interferometer and control beams, the difference between these two phase shifts $\phi_{ij} = \phi_{ij}^{ifo} - \phi_{ij}^{clf}$ can be non-zero. This relative phase shift gives rise to an offset in the lock point for the squeezing angle [25]:

$$\Delta\theta_{alignment} = \frac{\sum_{ij} \rho_{ij}^{clf} \rho_{ij}^{ifo} \sin\phi_{ij}}{1 + \sum_{ij} \rho_{ij}^{clf} \rho_{ij}^{ifo} \cos\phi_{ij}} \approx \sum_{ij} \rho_{ij}^{clf} \rho_{ij}^{ifo} \sin\phi_{ij}. \quad (5)$$

$\rho_{ij}^{ifo}, \rho_{ij}^{clf}$ are the ratio of the amplitudes of the TEM_{ij} to TEM_{00} spatial modes for the two fields. Here, we have assumed that both fields are dominated by the TEM_{00} mode, so that the summation in the denominator may be neglected. When both fields are very well aligned, the

lock point error is small and any coupling of alignment jitter to the measured quadrature phase is second order. However, when a static misalignment is present in one of the fields, the coupling is linear and the resulting quadrature fluctuations can be significant. Assuming that the control field is misaligned, we may linearise the above equation and express the quadrature fluctuations as:

$$\delta\theta_{sqz}(t) \approx \sum_{ij} \bar{\rho}_{ij}^{clf} \delta\rho_{ij}^{if_o} (1 + \bar{\phi}_{ij}) \delta\phi_{ij}(t) \quad (6)$$

Here $\bar{\rho}_{ij}^{clf}$ and $\bar{\phi}_{ij}$ result from a static misalignment of the control field and $\delta\rho_{ij}^{if_o}$ and $\delta\phi_{ij}^{if_o}$ arise due to jitter in the alignment of the interferometer beam. Alignment jitter can be a crippling source of quadrature fluctuations, and was measured to contribute 35 to 100 mrad depending on the alignment in the H1 experiment [12].

5. Backscattered light noise

When integrating a squeezed vacuum source into a gravitational wave detector, the OPO becomes a source of scattered light. Imperfections in the output Faraday isolator allow a small fraction of the light exiting the interferometer to travel towards the squeezed vacuum source, and a part of it is scattered back towards the interferometer. Relative motion between the scattering surface and the suspended interferometer optics generates phase fluctuations on the back-scattered light which will interfere with the signal field and add noise to the gravitational wave signal [14].

For an OPO motion δz_{sc} which is small compared to the wavelength λ , the relative intensity noise (RIN) due to scattered light at the interferometer output (RIN_{sc}) relative to quantum noise (RIN_{qn}) scales linearly with δz_{sc} [25]:

$$\frac{RIN_{sc}}{RIN_{qn}}(f) = 4\pi\delta z_{sc}(f) \sqrt{\frac{\eta_{PD}P_{sc}}{\lambda hc}} \quad (7)$$

where λ is the laser light wavelength, η_{PD} is the quantum efficiency of the readout photodiode, h and c are the Planck constant and speed of light, and P_{sc} is the backscattered power that reaches the output photodetector. P_{sc} can be explicitly written as:

$$P_{sc} = P_{sc,inc} R_{OPO} \eta_{loss} \quad (8)$$

where $P_{sc,inc}$ is the carrier power from the anti-symmetric port which is incident on the OPO, R_{OPO} is the reflection coefficient of the OPO, and η_{loss} accounts for propagation losses between the OPO and the readout photo-detector.

Backscattered light from the OPO can also degrade the interferometer sensitivity through non-linear couplings which up-convert low frequency noise into the gravitational wave band. These processes are nonstationary and can prevent gravitational wave detectors from reaching shot noise limited performance in their most sensitive band around 150 Hz. They will be even more harmful in advanced detectors where quantum noise limits the sensitivity down to 10 Hz (see [26] and references therein). We therefore require scattered light noise to be at least a factor of 10 below quantum noise over the entire aLIGO detection band, down to 10 Hz, to have enough margin to account for non stationarity. With squeezing enhancement, quantum noise will be reduced by a factor of $10^{s/20}$, where s is the level of noise reduction due to squeezing in decibels (dB). Thus, we impose:

$$\frac{RIN_{sc}}{RIN_{qn}}(f) = 4\pi\delta z_{sc}(f) \sqrt{\frac{\eta_{PD}P_{sc}}{\lambda hc}} \leq \frac{10^{s/20}}{10}. \quad (9)$$

Here we make the optimistic assumption that squeezing enhancement will be obtained over the entire frequency band. More realistically, the quantum noise reduction below 50 Hz will be significantly less than at high frequencies [15, 27].

From Eqs. 8 and 9, it is clear that there are three ways of minimizing the impact of scattered light: minimizing the OPO reflection coefficient R_{OPO} , decreasing the amount of light from the interferometer incident on the OPO cavity $P_{sc,inc}$, and reducing the motion of the OPO δz_{sc} . In first generation detectors, the LIGO H1 squeezing experiment employed a travelling wave OPO cavity design to obtain 50 dB of intrinsic power isolation, $R_{OPO} = 10^{-5}$ [28]. A Faraday isolator between the squeezed light source and the interferometer (see Fig. 2, top panel) further reduces the amount of spurious light reaching the squeezed light source. As shown in [14], even with this amount of optical isolation, the squeezing set-up employed during the LIGO H1 experiment would not meet the noise requirements for Advanced LIGO. GEO600 adopted a linear OPO cavity, relying exclusively on Faraday isolators for spurious light attenuation. In principle, a cascade of Faraday isolators could be inserted in Advanced LIGO between the Output Faraday and the OPO to reduce $P_{sc,inc}$. However, this approach has the downside of introducing additional losses in the squeezing injection path, and potentially introduces back scattered light noise from the Faraday isolators themselves.

6. Squeezing injection for future detectors

The maximum benefit from squeezing in future detectors can be achieved by minimizing the impact of all the noise sources described above. The Advanced LIGO case will be addressed here, but the analysis that follows can be applied to other advanced detectors.

6.1. Lowering optical losses

Table 1 summarizes the “expected” optical losses that the squeezed beam would experience in Advanced LIGO, given the interferometer optical components currently being installed. The total losses will realistically be between 20% and 30%, limiting the maximum amount of effective squeezing to 6 dB. However, several techniques to reduce optical losses are currently under investigation. The light coupling through the OMC can be improved by actively controlling the mode matching [29, 30], and a similar approach can be used to mode match the squeezed beam to the interferometer. Moreover, studies of scatter losses in fused silica optics and resonant cavities can be used to maximize the throughput of the Faradays isolators and the OMC [31, 32]. These techniques have the potential to reduce the total optical losses down to 10% - 15%.

6.2. Housing the OPO in the interferometer vacuum enclosure

Optical losses as low as 10% open up the possibility of achieving up to 10 dB of squeezing enhancement provided that quadrature fluctuations, backscattered light noise, and losses induced by misalignments are also reduced. We propose housing the OPO cavity on a seismically and acoustically isolated platform in vacuum in order to address these issues. To enhance the rigidity and length stability of the OPO, the optical elements can be bounded to a glass breadboard as for the Advanced LIGO OMC [38], while maintaining a bow-tie geometry [28].

In Advanced LIGO, the interferometer readout path (which includes the output Faraday and OMC) is placed on seismically isolated platforms within the main vacuum envelope (see Fig. 2). These platforms are large enough to accommodate the OPO and the entire squeezing injection path as well. This allows for a compact design which limits the number of optical components (each being a potential scatterer or source of loss) needed to route the squeezed beam to the interferometer output Faraday isolator.

A monolithic OPO which is seismically and acoustically isolated will have very little length noise. The noise performance should be comparable to the OMC cavities used in advanced

Table 1: *Expected* sources of loss for squeezing injection in Advanced LIGO (left), compared to *projected* losses achievable in the near future after replacing lossy Faraday rotators and polarizers, implementing active mode matching control, and reducing losses in the OMC.

Loss Source	Estimated	Projected
OPO	2%	2%
Squeezing injection optics	1%	1%
Squeezing injection Faraday	3% - 5%	0% - 2%
Output Faraday in Reverse	3% - 5%	1% - 2%
Mode matching (squeezed beam to interferometer)	4% - 6%	1% - 2%
Alignment fluctuations (squeezed beam to interferometer)	0% - 1%	0% - 1%
Total injection losses	10% - 18%	5% - 9%
Output Faraday	3% - 5%	1% - 2%
OMC transmission	3% - 6%	1% - 2%
Mode matching (interferometer to OMC)	4% - 6%	2% - 3%
Photo-detector	1%	1%
Total readout losses	10% to 17%	5% - 9%
Total losses	20% - 32%	9% - 17%

LIGO, which are designed to have less than $1 \times 10^{-15} m/\sqrt{Hz}$ of length noise at 100 Hz and above [38]. Below 100 Hz, the length noise of monolithic cavities typically scales as $1/\sqrt{f}$ [39]. Therefore, we expect an RMS length noise of $10^{-12} m$. Assuming that the optical parameters are identical to those used during the LIGO squeezing experiment, the OPO will generate 90 mrad of quadrature fluctuations per nanometer of RMS length noise [13], and thus will contribute less than 0.1 mrad RMS of phase noise. Squeezed quadrature fluctuations due to OPO length noise become negligible, and the resulting lock point errors in the coherent control scheme described in 4.1 become unimportant.

With a length noise of $1 \times 10^{-15} m/\sqrt{Hz}$ at 100 Hz, an in-vacuum OPO becomes a good frequency reference. For an OPO cavity length $l = 20$ cm, the frequency noise $\delta\nu$ for $\lambda = 1.064 \mu m$ laser light ($\nu = c/\lambda = 2.8 \times 10^{14}$) is:

$$\delta\nu = \frac{\nu}{l} \delta l \sim 1 \frac{Hz}{\sqrt{Hz}} \text{ at } 100 \text{ Hz} \quad (10)$$

This performance is comparable to a typical reference cavity. As a result, the error signal used to lock the OPO will be more sensitive to phase noise on the incoming pump field. The control topology of the OPO length servo can be modified by adding high bandwidth feedback to the pump laser frequency to suppress this noise. Although the pump laser itself is already stabilized by phase locking it to the interferometer laser (as depicted in Fig. 2), additional sources of phase noise exist on the pump path, such as length noise on the SHG cavity. Suppressing this noise is desirable, as it too will couple to the squeezed quadrature angle.

Additionally, housing the OPO and all of the injection optics in an acoustically and seismically isolated environment will reduce alignment jitter on the injected squeezed field. Typical mechanical resonances of seismically isolated optics are below 10 Hz, within the bandwidth of an automatic alignment system [35].

A simplified schematic of the proposed implementation of squeezing in Advanced LIGO with the OPO in vacuum is shown in the bottom panel of Fig. 2.

6.3. Squeezing angle sensing in transmission through the OMC

GEO600 recently established and implemented a new control scheme where the squeezing angle error signal is derived in transmission through the OMC to provide an improved error signal to shot noise ratio [33, 34]. We explicitly show here how the attenuation of higher order mode content by the OMC reduces the quadrature fluctuations and lock point errors due to misalignment (see Appendix A for a detailed derivation). Eqs. (5) and (6) may be rewritten in transmission through the OMC as:

$$\Delta\theta_{alignment}^{trans} \approx \sum_{ij} A_{ij} \rho_{ij}^{clf} \rho_{ij}^{ifo} \sin\phi_{ij} \quad (11)$$

$$\delta\theta_{sqz}^{trans}(t) \approx \sum_{ij} A_{ij} \bar{\rho}_{ij}^{clf} \delta\rho_{ij}^{ifo} (1 + \bar{\phi}_{ij}) \delta\phi_{ij}(t) \quad (12)$$

These equations are identical to Eqs. (5) and (6) with an additional factor, A_{ij} which accounts for the attenuation of higher order modes by the OMC.

The filtering of higher order modes by the Advanced LIGO OMC provides a 100-fold reduction in the coupling of alignment jitter to the squeezed quadrature angle (see Table 2 in Appendix A), making this noise source negligible.

6.4. Back scattering noise mitigation

In order to minimize backscatter, we propose maintaining the bow-tie geometry for the OPO cavity which provides 50 dB isolation from light exiting the squeezing injection port [28]. Moreover, placing this cavity on a seismically isolated platform will greatly reduce the OPO motion. In Advanced LIGO, isolated platforms provide a factor of 100 isolation from ground motion at frequencies above 1 Hz [42]. Figure. 3 shows plausible projections for back scattered light noise in a squeezing enhanced Advanced LIGO detector, calculated using Eqs. (7) and (8). Here we assume 100 mW interferometer light reaching the anti-symmetric port and 80 dB isolation in the path from the anti-symmetric port to the squeezed light source and back to the interferometer (30 dB isolation from the Output Faraday Isolator toward the squeezing injection path, and 50 dB isolation from the OPO itself).

We analyze three cases:

- OPO placed on a optics table with no seismic isolation, with a Squeezing Injection Faraday Isolator placed between the interferometer Output Faraday Isolator and the squeezing source (providing an additional 30 dB isolation);
- OPO placed in-vacuum on a seismically isolated platform, with a Squeezing Injection Faraday Isolator placed between the interferometer Output Faraday Isolator and the squeezing source (providing an additional 30 dB isolation);
- OPO *suspended* in-vacuum on a seismically isolated platform, without a Squeezing Injection Faraday isolator.

The curves in Fig. 3 confirm that placing the OPO on an optics table without seismic isolation would not meet the Advanced LIGO requirements below 200 Hz without inserting additional Faraday isolators which would increase the optical losses. Moving the OPO onto a seismic isolated platform will meet the back scattered light noise requirements above 30 Hz, and it might be acceptable at low frequencies depending on the actual OPO seismic motion and the amount of squeezing measured at low frequency with realistic filter cavities [15]. Suspending the OPO by a single stage suspension (1 Hz pendulum) would reduce the back scattered noise below requirements without the need for a Squeezing Injection Faraday Isolator. All the steering optics in the squeezing injection path would need similar vibrational isolation.

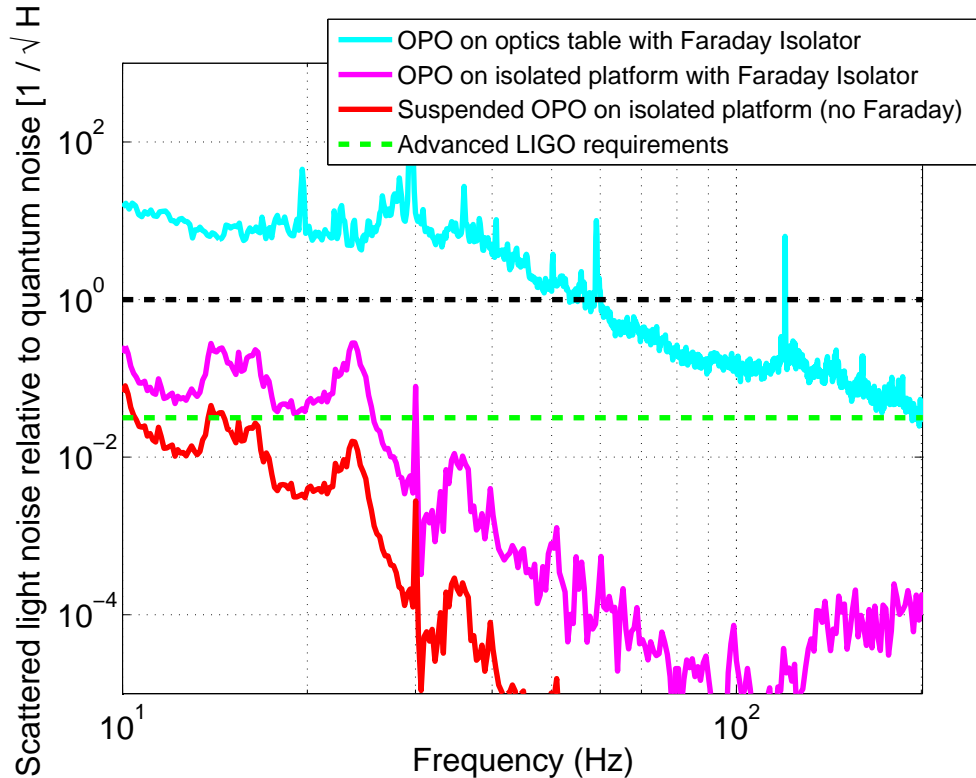


Fig. 3: Back scattered light noise projections for three different scenarios: OPO placed on an optics table on the ground, without seismic isolation (similar to the LIGO H1 squeezing demonstration setup [14]), OPO placed on an isolated platform enclosed in the main LIGO vacuum envelope [42]; OPO *suspended* on an isolated platform enclosed in the main LIGO vacuum envelope (a single stage 1 Hz suspension on an isolated platform is considered here). In the first two cases, 30 dB of isolation from spurious light reaching the OPO is also assumed. The requirement curve optimistically targets 10 dB of broadband squeezing.

7. Conclusion

We have identified some of the most significant barriers to achieving high levels of squeezing in future gravitational wave detectors, and have proposed solutions to overcome them. Specifically, we show how that there are three major deterrents: losses arising from optical components, from mode matching, and from misaligned optical beams; quadrature fluctuations due to length noise in the OPO and alignment jitter and noise arising from backscattered light. We quantified the contributions from each of these imperfections to the overall performance of a gravitational wave detector like Advanced LIGO, and we show how an in-vacuum OPO, together with an improved control scheme can minimize the impact of all of these noise sources. Housing the OPO in vacuum, using the OMC transmission to derive a better error signal for quadrature fluctuations, and introducing additional alignment and mode-matching control [29, 30, 35] will also increase the operational reliability of the squeezed light source. These proposed solutions, when coupled with quantum noise filter cavities [15], promise to deliver up to 10 dB of squeezing enhancement across a broad range of frequencies critical to future gravitational wave detectors.

A. Calculation of squeezed quadrature lock point errors due to misalignment

As described in section 4, the coherent control scheme used in all squeezed vacuum sources deployed at gravitational wave detectors to date is used to stabilize two phases. An error signal derived in reflection from the OPO is used to stabilize the phase difference between the two control sidebands $\psi = \phi^+ - \phi^-$. Setting ϕ^+ equal to zero for simplicity, the phase of the second control sideband generated in the OPO, ϕ^- , is equal to the phase of the pump field θ_B . At the interferometer output, a second error signal is derived to stabilize the phase between the control and interferometer fields $\phi = \phi^+ - \phi^{ifo}$. Stabilizing these two phases locks the relative phase between the squeezed field and the interferometer beam, or *squeezing angle*:

$$\theta_{sqz} = \theta_B/2 - \phi^{ifo} = \phi - \psi/2 \quad (13)$$

In general, the interferometer and control fields at the detector output can both be misaligned and contain some higher order mode content. For the remainder of this analysis, I will expand both fields in terms of the TEM_{ij} eigenmodes of the interferometer OMC cavity. In the presence of higher order modes, the error signal used to lock ϕ , after demodulation at the control frequency Ω and low pass filtering, can be expressed as [25]:

$$I_{err} \propto a_{00}^{ifo} a_{00}^+ \cos(-\phi + \theta_{dm}) + a_{00}^{ifo} a_{00}^- \cos(\phi - \psi + \theta_{dm}) \\ + \sum_{ij} a_{ij}^{ifo} \left[a_{ij}^+ \cos(-\phi + \phi_{ij}^{ifo} - \phi_{ij}^+ + \theta_{dm}) + a_{ij}^- \cos(\phi - \psi + \phi_{ij}^- - \phi_{ij}^{ifo} + \theta_{dm}) \right] \quad (14)$$

Above, a_{ij}^{ifo} , a_{ij}^+ , and a_{ij}^- represent the norm of the electric field amplitude for the TEM_{ij} component of the interferometer and control fields respectively and θ_{dm} is the demodulation phase. Here, ϕ_{ij}^{ifo} , ϕ_{ij}^+ , and ϕ_{ij}^- are the phase shifts between the TEM_{00} and TEM_{ij} modes for the interferometer and control fields. When we derive the error signal from the fields incident on the OMC, we can make a few simplifications to eq. 14.

$$I_{err} \propto \cos(-\phi + \theta_{dm}) + \alpha \cos(\phi - \psi + \theta_{dm}) \\ + \sum_{ij} \rho_{ij}^{ifo} \rho_{ij}^{clf} [\cos(-\phi + \phi_{ij} + \theta_{dm}) + \alpha \cos(\phi - \psi - \phi_{ij} + \theta_{dm})] \quad (15)$$

In this case the phases ϕ_{ij}^+ and ϕ_{ij}^- are equal and we will express both as ϕ_{ij}^{clf} as was done in section 4.2. The factors ρ_{ij}^{ifo} , ρ_{ij}^{clf} , and ϕ_{ij} , are identical to those in section 3 as well:

$$\rho_{ij}^{ifo} = \frac{a_{ij}^{ifo}}{a_{00}^{ifo}} \quad \rho_{ij}^{clf} = \frac{a_{ij}^+}{a_{00}^+} \quad \phi_{ij} = \phi_{ij}^{ifo} - \phi_{ij}^{clf} \quad (16)$$

In 14, we have pulled out a common factor of $a_{00}^{ifo} a_{00}^+$ from all terms. We have also used the fact that the ratio of the amplitudes of the two control sidebands is the same in all spatial modes to make the following substitution:

$$\alpha = \frac{a_{00}^+}{a_{00}^{ifo}} = \frac{a_{ij}^-}{a_{ij}^+} \quad (17)$$

Note that the expression on the first line of Eqs. 14 and 15 is the error signal in the absence of higher order mode content. We tune θ_{dm} so that the first line is zero when ϕ and ψ correspond to the desired squeezing angle. For interferometers using DC readout, [37] we desire amplitude

squeezing at the output and set $\theta_{dm} = \psi/2 - \pi/2$ so that the error signal is zero when $\phi = \pi/2 + \theta_{dm}$ and $\theta_{sqz} = 0$. Now we include a small misalignment such that $a_{ij} \ll a_{00}$ for all fields. When we lock and $I_{err} = 0$, then $\phi \approx \pi/2 + \theta_{dm} + \Delta\phi$ where $\Delta\phi$ is a small angle. Plugging these phases into Eq. 15, we obtain:

$$I_{err} \propto -(1 - \alpha) \left[\sin(\Delta\phi) + \sum_{ij} \rho_{ij}^{if_o} \rho_{ij}^{cl_f} \sin(\Delta\phi - \phi_{ij}) \right] \quad (18)$$

We can then solve for the lock point error $\Delta\phi$ by setting $I = 0$ and using the small angle approximation to first order. This gives us Eq. 5, which we have restated below for clarity:

$$\Delta\phi = \frac{\sum_{ij} \rho_{ij}^{cl_f} \rho_{ij}^{if_o} \sin\phi_{ij}}{1 + \sum_{ij} \rho_{ij}^{cl_f} \rho_{ij}^{if_o} \cos\phi_{ij}} \approx \sum_{ij} \rho_{ij}^{cl_f} \rho_{ij}^{if_o} \sin\phi_{ij} \quad (19)$$

Since it is the presence of higher order modes which leads to lock point errors, it is desirable to derive the error signal in transmission through the OMC in order to filter out higher order mode content. We proceed to calculate the lock point errors in this case by returning to 14 and including the effect of the cavity on all phases and field amplitudes. Note that many of the assumptions made in deriving Eq. 15 are no longer valid once the fields pass through the OMC. The field amplitudes are modified as follows:

$$\begin{aligned} a_{00,tr}^{if_o} &= T(0) a_{00}^{if_o} & a_{ij,tr}^{if_o} &= T(\Delta\omega(i,j)) a_{ij}^{if_o} \\ a_{00,tr}^+ &= T(\Omega) a_{00}^+ & a_{ij,tr}^+ &= T(\Omega + \Delta\omega(i,j)) a_{ij}^+ \\ a_{00,tr}^- &= T(-\Omega) a_{00}^- & a_{ij,tr}^- &= T(-\Omega + \Delta\omega(i,j)) a_{ij}^- \end{aligned} \quad (20)$$

Here, $T(\omega)$ is the cavity amplitude transmission for a field with detuning ω and $\Delta\omega(i,j)$ is the frequency shift of the cavity resonance for the TEM_{ij} mode. In order to simplify our expressions for the phases, we will treat the case where the OMC cavity is linear and note that generalizing to the case of a travelling wave cavity is straightforward. Assuming that the control side-bands are well outside of the cavity linewidth, the phase shifts in transmission are:

$$\begin{aligned} \phi_{tr}^{if_o} &= \phi^{if_o} & \phi_{tr}^+ &= \phi^+ - \pi/2 & \phi_{tr}^- &= \phi^- + \pi/2 \\ \psi_{tr} &= \psi - \pi & \phi_{tr} &= \phi - \pi/2 & \theta_{sqz,tr} &= \theta_{sqz} \end{aligned} \quad (21)$$

We also assume that the first several higher order modes are well outside of the cavity linewidth and lie above the cavity resonance:

$$\phi_{ij,tr}^{if_o} = \phi_{ij}^{if_o} - \pi/2 \quad \phi_{ij,tr}^+ = \phi_{ij}^+ - \pi/2 \quad \phi_{ij,tr}^- = \phi_{ij}^- - \pi/2 \quad (22)$$

Plugging Eqs. 20 and 21 into Eq. 14 and simplifying yields:

$$\begin{aligned} I_{err} &\propto \cos(-\phi_{tr} + \theta_{dm}) + \alpha \cos(\phi_{tr} - \psi_{tr} + \theta_{dm}) + \sum_{ij} \frac{T(\Delta\omega(i,j))}{T(\Omega)} \rho_{ij}^{if_o} \rho_{ij}^{cl_f} \\ &\times [\cos(-\phi_{tr} + \phi_{ij} + \theta_{dm}) T(\Omega + \Delta\omega(i,j)) + \alpha \cos(\phi_{tr} - \psi_{tr} - \phi_{ij} + \theta_{dm}) T(-\Omega + \Delta\omega(i,j))] \end{aligned} \quad (23)$$

We proceed as before and set $\theta_{dm} = \psi_{tr}/2 - \pi/2$ and $\phi_{tr} \approx \pi/2 + \theta_{dm} + \Delta\phi$. Again we set $I = 0$ and make the small angle approximation to first order and solve for $\Delta\phi$ to obtain:

$$\Delta\phi \approx \sum_{ij} A_{ij} \rho_{ij}^{ifo} \rho_{ij}^{clf} \sin(\phi_{ij})$$

$$A_{ij} = \frac{T(\Delta\omega(i, j))}{(1 - \alpha)T(\Omega)} [T(\Omega + \Delta\omega(i, j)) - \alpha T(-\Omega + \Delta\omega(i, j))] \quad (24)$$

Table 2 shows the values of A_{ij} for the first 10 sets of higher order modes using the parameters for the advanced LIGO OMC. We see that the reduction in the coupling of alignment jitter to quadrature fluctuations typically exceeds two orders of magnitude.

Table 2: Coupling coefficients A_{ij} calculated using the parameters for the advanced LIGO OMC. This cavity has a finesse of 390, higher order mode spacing of 58 MHz, and a free spectral range of 264.8 MHz. The detuning of the control sidebands, Ω , is 15 MHz. A mode order of n corresponds to any mode TEM_{ij} with $i + j = n$.

mode order	1	2	3	4	5
A_{ij}	0.0012	0.00071	0.0011	0.0086	0.0080

mode order	6	7	8	9	10
A_{ij}	0.00086	0.00075	0.0020	0.11	0.0014

For a higher order modes with large values of i and j $\Delta\omega(i, j)$ will eventually be comparable to the OMC cavity free spectral range. If all fields are still well outside of the cavity linewidth but the two control side-bands lie on opposite sides of a cavity resonance, one of the two ϕ_{ij} 's in Eq. 23 will pick up a factor of π resulting in the corresponding term in A_{ij} picking up a minus sign. If one of the fields becomes close to the cavity resonance, the approximations in Eqs. 21 and 22 may break down. However, it typically is possible to design the OMC and pick Ω such that this will not happen until the mode order is quite large. It is then a reasonable approximation to terminate the sum in Eq. 24 before this becomes a problem and the result derived above remains valid.

Acknowledgments

The authors gratefully acknowledge our collaborators within the LIGO Scientific Collaboration (LSC) working on quantum noise research at the Australian National University and at the University of Hannover, in particular Hartmut Grote for comments about this manuscript. We also thank our colleagues at the LIGO Laboratory, John Miller, Matthew Evans and Peter Fritschel, for insightful discussions and comments about this manuscript. We are grateful to the National Science Foundation for generous support of this work under the LIGO cooperative agreement PHY-0757058. This research was supported in part by an award to E.O. from the Department of Energy (DOE) Office of Science Graduate Fellowship Program (DOE SCGF) administered by Oak Ridge Associated Universities (ORAU) under DOE contract number DE-AC05-06OR23100. The DOE SCGF Program was made possible in part by the American Recovery and Reinvestment Act of 2009. This paper has the LIGO document number LIGO-P1400064.